A General Description of Detachment for Multidimensional Modelling of Biofilms

Joao de Bivar Xavier, Cristian Picioreanu, Mark C.M. van Loosdrecht

Department of Biotechnology, Delft University of Technology, Julianalaan 67, 2628 BC Delft, The Netherlands; telephone: +31 (0)15 2781551; fax: +31 (0)15 2782355; e-mail: j.xavier@tnw.tudelft.nl

Received 3 January 2005; accepted 9 March 2005

Published online 25 May 2005 in Wiley InterScience (www.interscience.wiley.com). DOI: 10.1002/bit.20544

Abstract: A general method for describing biomass detachment in multidimensional biofilm modelling is introduced. Biomass losses from processes acting on the entire surface of the biofilm, such as erosion, are modelled using a continuous detachment speed function F_{det}. Discrete detachment events, i.e. sloughing, are implicitly derived from simulations. The method is flexible to allow F_{det} to take several forms, including expressions dependent on any state variables such as the local biofilm density. This methodology for biomass detachment was integrated with multidimensional (2D and 3D) particle-based multispecies biofilm models by using a novel application of the level set method. Application of the method is illustrated by trends in the dynamics of biofilms structure and activity derived from simulations performed on a simple model considering uniform biomass (case study I) and a model discriminating biomass composition in heterotrophic active mass, extracellular polymeric substances (EPS) and inert mass (case study II). Results from case study I demonstrate the effect of applied detachment forces as a fundamental factor influencing steady-state biofilm activity and structure. Trends from experimental observations reported in literature were correctly described. For example, simulation results indicated that biomass sloughing is reduced when erosion forces are increased. Case study II illustrates the application of the detachment methodology to systems with non-uniform biomass composition. Simulations carried out at different bulk concentrations of substrate show changes in biofilm structure (in terms of shape, density and spatial distribution of biomass components) and activity (in terms of oxygen and substrate consumption) as a consequence of either oxygen-limited or substrate-limited growth.
Keywords: biofilm; detachment; erosion; sloughing; individual-based modelling; EPS; level set

INTRODUCTION

Biomass detachment, i.e. the interphase transport of biomass particles from an attached microbial film to the fluid compartment bathing the film (Stewart, 1993), is often the primary process balancing biofilm growth in biofilm reactors (Van Loosdrecht et al., 1995). Detachment determines the steady state accumulation of the biofilm and the average solids retention time (SRT) of the system and is a key parameter influencing biofilm composition and activity (Morgenroth and Wilderer, 1999, 2000). Hence, knowledge and control of biomass detachment is of chief importance in the operation of a biofilm reactor (Tijhuis et al., 1996).

Biomass detachment in biofilms may be caused by a diversity of mechanisms including erosion, sloughing, abrasion, predator grazing and human intervention (Bryers, 1988). However, in spite of the diverse causes of detachment, for modelling purposes a simple description using overall detachment rates may be sufficient to explain experimental observations (Stewart, 1993). Wanner and Gujer (1986) included a generic detachment description in their multispecies one-dimensional (1D) biofilm model, later implemented in the AQUASIM software (Reichert, 1994). This approach describes detachment using a detachment velocity, i.e. the speed at which the biofilm front retracts as a consequence of biomass detachment, allowing almost any function of time (or other relevant physical quantity) to be used as the detachment function. Applications of this approach include for example the interpretation of experimental biofilm results (Horn et al., 2003) and a theoretical study on the influence of detachment mechanisms on competition in biofilms (Morgenroth and Wilderer, 2000).

Apart from the processes involved in detachment, a large number of processes are involved in biofilm formation (Characklis and Marshall, 1990). Therefore, mathematical modelling of biofilm activity is a highly complex task. 1D approaches, such as the model of Wanner and Gujer, simplify this task by restricting the variation of the state variables to a single direction perpendicular to the surface of the solid carrier (often called the ''vertical'' direction). This is a valid simplification when vertical gradients are orders of magnitude higher than those in the directions parallel to the carrier surface (Wanner and Gujer, 1986), the ''horizontal'' directions. Since this applies to most biofilm systems, dynamic multispecies 1D biofilm models are sufficient for the majority of practical purposes (Van Loosdrecht et al., 2002). However, 1D models are not able to describe the dynamics of biofilm

Correspondence to: Joao de Bivar Xavier
Contract grant sponsor: F.C.T./M.C.T.E.S., Portugal
Contract grant number: SFRH/BPD/11485/2002

activity in cases where structural dependent factors, such as external mass transfer coefficient or biofilm porosity, change significantly in time. This is, for instance, the case of the decrease of biofilm activity caused by irregular biofilm surface and heterogeneous structures, which requires two dimensional (2D) or three dimensional (3D) descriptions (Eberl et al., 2000; Klapper, 2004; Picioreanu et al., 2000a).

Merits of multidimensional (2D or 3D) biofilm modelling, in particular bottom-up approaches, include the ease to which they may be used to describe numerous processes involved in biofilm formation based on first principle descriptions (Van Loosdrecht et al., 2002). Bottom-up biofilm models are approaches where the large-scale dynamics are emergent from the processes occurring at a small-scale. These approaches are fundamentally different from continuum methods, which use a homogeneous representation of the biomass and differential equations widely used in physics to model the dynamics of biomass spreading (Alpkvist et al., 2004; Dockery and Klapper, 2001; Eberl et al., 2001). Two bottom-up biofilm modelling approaches are presently found in the literature: cellular automata (CA) and individual-based modelling (IbM). These approaches mainly differ in the method used for representation of biomass. The CA-based biofilm models use the discretization of biomass along a grid (typically rectangular, e.g. Noguera et al., 1999; Picioreanu et al., 1998; Pizarro et al., 2001), whereas the IbM uses an agent-based approach where the biomass is represented by spherical particles (Kreft et al., 2001; Picioreanu et al., 2004).

The present study reports a general description of the methodology for modelling biomass detachment integrated with multidimensional modelling of biofilms. Previous methods for implementing detachment in 2D or 3D biofilm models have so far opted for specific descriptions of a particular detachment mechanism. The removal of biomass from the biofilm following a rate proportional to the local biomass composition (Noguera et al., 2000; Pizarro et al., 2001) or to the local concentration of a ''chemical detachment factor'' of bacterial origin (Hunt et al., 2003) were included in CA models. Although these studies reported the modelling of biomass detachment, the algorithms used allowed biomass removal to occur at any location within the biofilm. These procedures, in our view, should better be referred to as biomass decay, since they are not restricted to the interphase transport of biomass particles. Hermanowicz (2001) used in his CA model a stochastic method for the removal of biomass at the biofilm/liquid interface. Detachment occurred with a given probability, defined as function of an overall shear stress and parameter quantifying biofilm strength. Other models (Chang et al., 2003; Picioreanu et al., 2004) implemented the cutting off of any biomass reaching beyond a maximum biofilm thickness with the simple purpose of keeping the biomass within the computational domain. This method, in practice, imposes that the biofilm will have a flat shape at steady-state. Therefore, it may not be used if the purpose of the model is to investigate the dynamics of the biomass shape.

The most extensive description of biomass detachment proposed to this date was based on the mechanistic representation of hydrodynamic stress on the biofilm structure (Picioreanu et al., 2001). This model, implemented in 2D, used computational fluid dynamics (CFD) to determine the velocity profiles of the moving liquid and then calculated the propagation of stresses imposed on the biofilm structure, assumed to be an elastic material. Detachment occurred when stresses exceeded the local strength of the biofilm. The application of this method allowed the generation of realistic biofilm formation patterns correlated with the flow regime and the substrate load. More importantly, it provided a unified description of erosion and detachment, supporting the view that a distinction between these two phenomena may be arbitrary (Stewart, 1993), since in many systems there is a broad distribution of detached particle sizes (Choi and Morgenroth, 2003).

In spite of the merits of this approach, some limitations of the detachment model of Picioreanu et al. (2001) still raise the necessity for new models of biomass detachment for multidimensional modelling of biofilms. Application of the model was limited to the specific case of liquid flowing in a direction parallel to the solid substratum and in laminar regime. The method, requiring CFD computations at each iteration of the biofilm growth cycle, had the disadvantage of being computationally very demanding. Finally, it required knowledge of mechanical properties of the biofilm that is scarcely available. For practical purposes, a detachment model that is simple and still allows deriving the influence of detachment forces on the dynamics of biofilm structure and activity does not require a mechanistic approach. Such a simple and general method should be flexible enough to allow the modelling of diverse detachment scenarios. Furthermore, it should be numerically efficient so that its computational footprint is negligible relatively to the other, already demanding, operations performed in the course of multidimensional simulations.

A generic method to represent biomass detachment for multidimensional modelling of biofilms is proposed here. This detachment method is a multidimensional (2D and 3D) extension of the general description included in the 1D model of Wanner and Gujer (Wanner and Reichert, 1996). Similarly its 1D counterpart, the present method permits continuous detachment functions to be defined by practically any function of time and of relevant state variables (local or global), such as for example local biomass density or the local concentration of detachment-inducing chemical species. Therefore, the present method may be used to describe a diversity of detachment scenarios. This multidimensional extension further allows the unified modelling of biomass erosion and sloughing, similar to that implemented by the more complex mechanistic approach (Picioreanu et al., 2001). The present method is generic enough to allow its integration with both bottom-up and continuum approaches of multidimensional biofilm modelling. This study focuses on the integration of the detachment procedures with IbM. In Xavier et al. (2005) we have described the IbM framework in detail.

MATHEMATICAL DESCRIPTION OF BIOMASS DETACHMENT

The mathematical description of biomass detachment uses a detachment speed function, F_{det}, here defined as the speed of biofilm front retreat resulting from detachment mechanisms that act on the entire biofilm surface (e.g. erosion). $F_{det}(\mathbf{x})$, where $\mathbf{x}$ is a point located on the biofilm/liquid interface, is a speed in the direction normal to the surface of the biofilm/liquid interface (here called surface Γ) at that point, which is expressed by

$$\frac{d\mathbf{x}}{dt} = -F_{det}(\mathbf{x})\mathbf{n}(\mathbf{x}) \quad [LT^{-1}] \tag{1}$$

In Equation 1 $\boldsymbol{n}(\mathbf{x})$ is the vector normal to the surface at point $\mathbf{x}$. This is illustrated in the inset ''zoomed area (A*)'' shown in Figure 1. Equation 1 is here expressed independently of the dimensionality of the system, i.e. it is valid for both 2D (where $\mathbf{x}$ is defined in x and y coordinates) and 3D (where $\mathbf{x}$ is defined in x, y and z coordinates). Provided a function F_{det}, time course of the biofilm surface, Γ, is determined by solving Equation 1. F_{det} may have any form, namely it may vary spatially and temporarily according to almost any function of local or global state variables. For example, F_{det} can depend on measured biofilm mechanical properties, on local biomass EPS composition, on the distance to the solid support, *etc.* The detachment rates, as biofilm biomass lost per unit of area per time, will be therefore determined by the same factors included in F_{det}. Local detachment rates derived from this method are a function of the local curvature of the biofilm/liquid interface. Independently of the form of F_{det}, numerical simulations show that local detachment rates are higher in convex regions, such as the tips of protuberances, and lower in concave regions, such as the less exposed interior of pores. This feature is in agreement with the observations that detachment forces have more influence on the protuberances of heterogeneous biofilms (Van Loosdrecht et al., 1995). It should be noted that, when applied to 1D, Equation 1 becomes

$$-\frac{dL_f}{dt} = F_{det} \quad [LT^{-1}] \tag{2}$$

in which L_f (''length'' of film) is the position of the biofilm/liquid interface. Equation 2 is the approach used in the well-established 1D biofilm dynamic models (Wanner and Gujer, 1986; Wanner and Reichert, 1996) to describe surface detachment of biomass.

Equation 1 is solved numerically by a method adapted from the procedure for monotonically advancing fronts introduced by Sethian (1996). This solution method is applicable if

$$F_{det}(\mathbf{x}) > 0 \quad \text{for any location } \mathbf{x} \text{ in } \Gamma \tag{3}$$

The inequality (Eq. 3) simply states that any point in the biofilm/liquid interface is subject to a non-zero detachment speed. This is a realistic statement because local values of F_{det} may be made as small as necessary (i.e. very close to zero) for practical purposes when no detachment must take place. Negative values of F_{det}, which would mean biomass accumulation resultant from detachment, are not physically possible. By imposing constraint 3, Equation 1 may be written in the form

$$-F_{det}|\nabla T(\mathbf{x})| = 1 \quad [\text{dimensionless}] \tag{4}$$

where $T(\mathbf{x})$ is the time at which the interface Γ crosses a point $\mathbf{x}$ located inside the biofilm. Equation 4 is a form of the Eikonal equation and can be solved numerically in very efficient ways using the *fast marching level set method* (Sethian, 1996, 1999).

Given the function F_{det} and the biofilm structure, values for $T(\mathbf{x})$ may be determined for all points inside the biofilm. F_{det} may be a function of any form, derived for instance from the empirical detachment rates found in the literature (see Morgenroth and Wilderer, 2000 for a list). Such expressions, when reported in terms of detached mass per area of biofilm per time ($[M L^{-2} T^{-1}]$ units) may be converted to detachment speed ($[LT^{-1}]$ units) by dividing by the local biomass density.

The field of $T(\mathbf{x})$ values describe local evolution of the biofilm interface as a consequence of detachment forces effective to the entire biofilm surface, i.e. erosion, as illustrated in panels A and B of Figure 1. Surface detachment is then complemented with the removal of biomass that becomes disconnected from the biofilm after application of surface detachment. This removal of biomass clusters in discrete events allows representation of biofilm sloughing. Here, sloughing occurs when the base of attachment of biomass clusters disappears, as illustrated in pane C of Figure 1. It must be stressed that this description of sloughing events is not possible for 1D modelling using this method. In 1D modelling applications, the occurrence of sloughing events is commonly modelled using a list of programmed events (e.g. Horn et al., 2002; Morgenroth and Wilderer, 2000) rather than being implicitly derived from simulations. In 2D and 3D sloughing events are derived explicitly from the erosion processes, which is in accordance with the view that sloughing occurs by the same mechanisms as other detachment modes (Picioreanu et al., 2001; Stewart, 1993).

INTEGRATION WITH MULTIDIMENSIONAL MODELLING OF BIOFILM GROWTH

This paragraph explains how the detachment procedure was integrated with individual based modelling of biofilms (IbM). The method to apply IbM to biofilm modelling was described in detail previously (Kreft et al., 2001; Picioreanu et al., 2004; Xavier et al., 2005); only a brief description is provided here. In the IbM, biomass is represented as being composed by particles with a circular (if simulations are in 2D space) or spherical shape (if simulations are in 3D space). These particles, called ''agents'', are entities with an internal state defined by their composition (mass of one or more particulate substances), size and location in space (either in

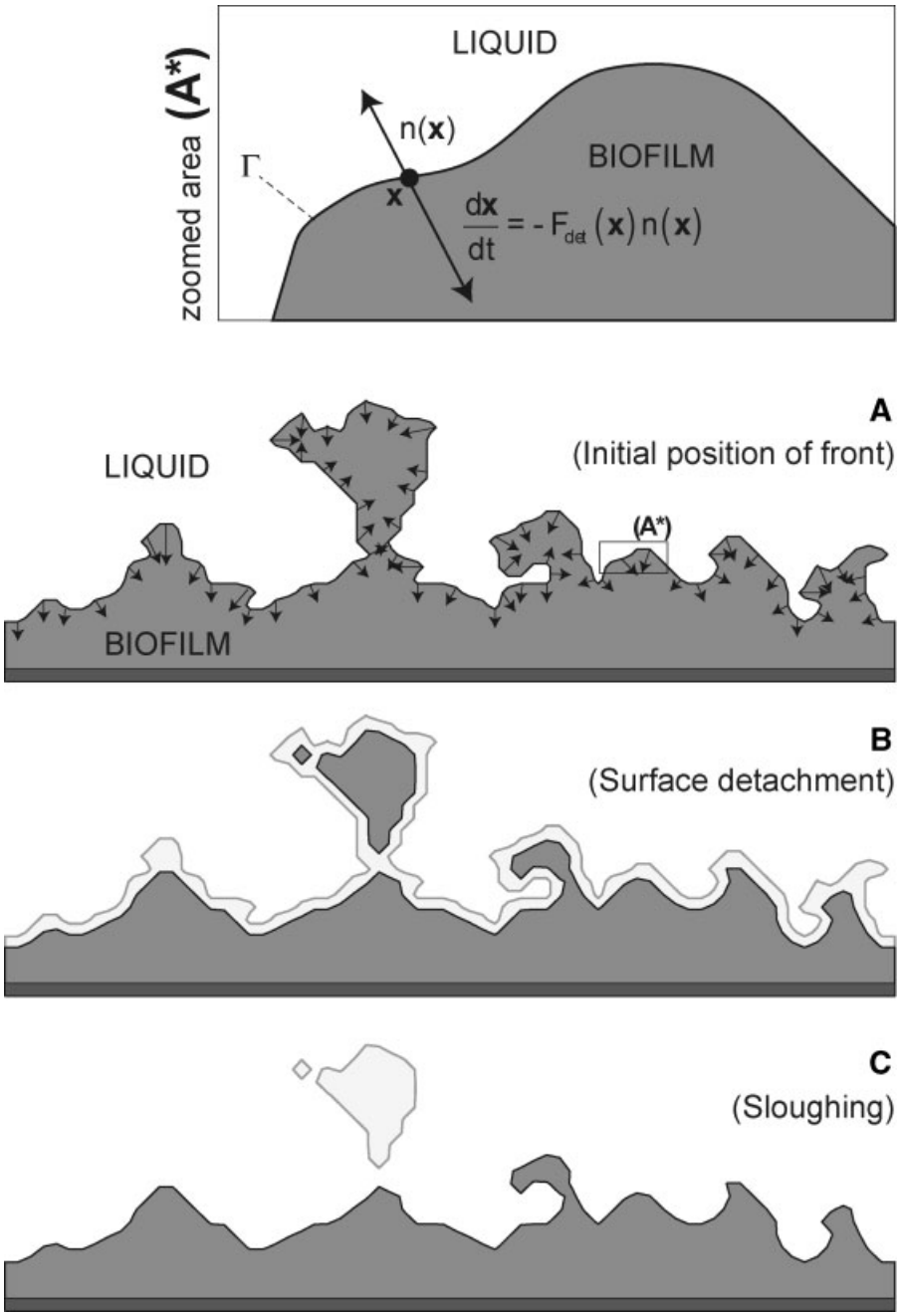

Figure 1. Schematic representation of the procedure for implementing biomass detachment. Inset **Zoomed A***—The surface detachment rate at a point (**x**) placed at the biofilm interface (Γ) results from the product of local values of the detachment speed function, F_{det}, and the vector normal to the surface at that point ($\boldsymbol{n}(\mathbf{x})$), as described by Equation 1. (**A**) shows the position of the biofilm front before detachment is applied (time t), with the detachment speed vectors (black arrows) represented at many points in the surface. (**B**) shows the surface after application of the surface detachment (time $t + \Delta t$). (**C**) biomass not connected to the biofilm is removed resulting in the loss of relatively large biomass clusters of biomass by sloughing.

2D or 3D). Agents follow behaviour rules that mimic the behaviour of a microbial cell: they grow by intake of nutrients, divide creating an offspring agent, move (in continuous spatial coordinates) when pushed by neighbouring agents and shrink if their biomass decreases by processes of decay. Growth (biomass production) and decay of agents are entirely defined in terms of reactions that observe principles of conservation of mass for the involved substrates and products. Model biofilm systems may consider any number of substrates and products for an arbitrary number of reactions occurring. Details for the model implementation in a computer software are given in Xavier et al. (2005). The model makes a distinction between particulate and solute species. Diffusion and reactions of the solute species in the system is modelled using an uncoupled approach (Picioreanu et al., 1998), where solute concentration fields are described using a rectangular grid. Particulate species are used to describe the composition of the biomass in the biofilm. The IbM is a bottom-up approach to biofilm modelling, since the rules are defined at the small-scale (i.e. the biomass

particle ''agent'') and the development of a biofilm and its features (structure and activity of the biofilm) are emergent properties.

Simulations carried out in the IbM use a computational cycle that consists of the sequential execution of operations that represent the processes involved in biofilm development. These operations are executed in the following order:

A. Growth and division of biomass
B. Spreading of the biofilm matrix
C. Detachment of biomass
D. Solving mass balances to determine bulk concentrations of solutes in the system
E. Solving steady state diffusion-reaction mass balances of solutes in the biofilm and in the mass transfer boundary layer.
F. Advancement of the present simulation time (t) to $t + \Delta t$ and return to step A to start a new iteration of the cycle, or stop the iteration if t reached the predefined simulation finishing time, t_{finish}

More details on the computational cycle and the determination of a suitable iteration time step (Δt) are given in Xavier et al. (2005). The step concerning the detachment of biomass implements the method described here. Since in the IbM the biomass is represented by a collection of particles, the first operation is the mapping of particle masses into a grid representation. The grid-based biomass distribution is required for the solution of Equation 4 using the level set method. Solving Equation 4 results in the determination of the $T(\mathbf{x})$ values for the biofilm structure. Figure 2 displays $T(\mathbf{x})$ values calculated for an example biofilm structure using four different F_{det} functions, illustrating the flexibility of the method. Following determination of $T(\mathbf{x})$, particles placed at locations with $T(\mathbf{x}) < \Delta t$ will be removed, implementing surface detachment in the time interval Δt. In order to have a detachment precision that is not limited to the grid size used for the biomass mapping, biomass particles located at the biofilm interface are further eroded by decreasing particle volume by a quantity ΔV determined from the local value of $T(\mathbf{x})$:

$$\Delta V_i = -\frac{\Delta t}{T(\mathbf{x})} V_i \quad [\mathrm{L}^3] \tag{5}$$

Finally, all biomass material not connected anymore to the solid surface is removed from the system, which simulates the occurrence of sloughing events.

As will be illustrated in the case studies reported here, the integration of the present detachment model with the IbM approach allows the achievement of a quasi steady state in biomass accumulation. The biofilm accumulation is derived by the model from a balance between growth and detachment rather than being explicitly imposed.

Inoculation of the System in Simulations

For all simulations reported here, the system was initialised with a single layer of biomass particles covering the totality of the solid substratum. The radius of the initial particles is the maximum radius of particles, which has values $R_{division} = 6$ μm for *case study I* and $R_{division} = 8$ μm for *case study II*. In practice, this corresponds to an initial state of a thin homogenous biofilm with thickness 12 and 16 μm for case studies *I* and *II*, respectively.

CASE STUDY I: STEADY STATE ACTIVITY AND STRUCTURE OF A BIOFILM

This case study uses a very simple kinetic model for biomass growth to illustrate how the multidimensional description of biomass detachment can be used to represent trends observed experimentally in the operation of biofilm reactors. The relation between biofilm structure/activity and the growth conditions in biofilm reactors has been extensively studied (Kinner et al., 1983; Kwok et al., 1998; Tijhuis et al., 1996; Wasche et al., 2002). It appeared that biofilm morphology in steady state operated biofilm reactors depends on a balance between biomass growth and detachment forces (Van Loosdrecht et al., 1995). It has been observed that (i) with increasing detachment forces, biofilms developed have a smoother surface and smaller thickness; (ii) higher mechanical stress applied in the biofilm produces biofilms that are less subject to sloughing, effectively decreasing sloughing rates and (iii) when sloughing is significant, the biofilm structure structural characteristics reach a ''noisy'' steady state (Morgenroth and Wilderer, 2000).

Model Description

To describe the experimental observations listed above, a simple model representation of biomass with uniform density and composition is sufficient. The model biomass is composed by a single particulate species, heterotrophic active mass. Also for simplicity of the analysis it is considered that a single solute species (oxygen) is growth limiting for the heterotrophic organisms. The rate of production of heterotrophic biomass, R_H, follows a Monod type of kinetics in relation to the concentration of oxygen, C_O

$$R_H = \mu^{max} \frac{C_O}{K_O + C_O} C_H \quad [\mathrm{M_H L^{-3} T^{-1}}] \tag{6}$$

where μ^{max} is the maximum specific growth rate of biomass, K_O is the half-saturation constant for oxygen and C_H is the concentration of heterotrophic biomass. The reaction rate of oxygen, R_O, derives from the biomass production rate multiplied by the yield coefficient, Y_{OH}, and is negative since oxygen is consumed during growth:

$$R_O = -Y_{OH} R_H \quad [\mathrm{M_O L^{-3} T^{-1}}] \tag{7}$$

Detachment by erosion is here modelled using a speed of detachment that is a function of the square of the distance to the solid substratum, x

$$F_{det}(\mathbf{x}) = k_{det} x^2 \quad [\mathrm{LT^{-1}}] \tag{8}$$

where k_{det} (having dimensions of $\mathrm{L^{-1}T^{-1}}$) is the detachment speed coefficient. A second-order dependence on

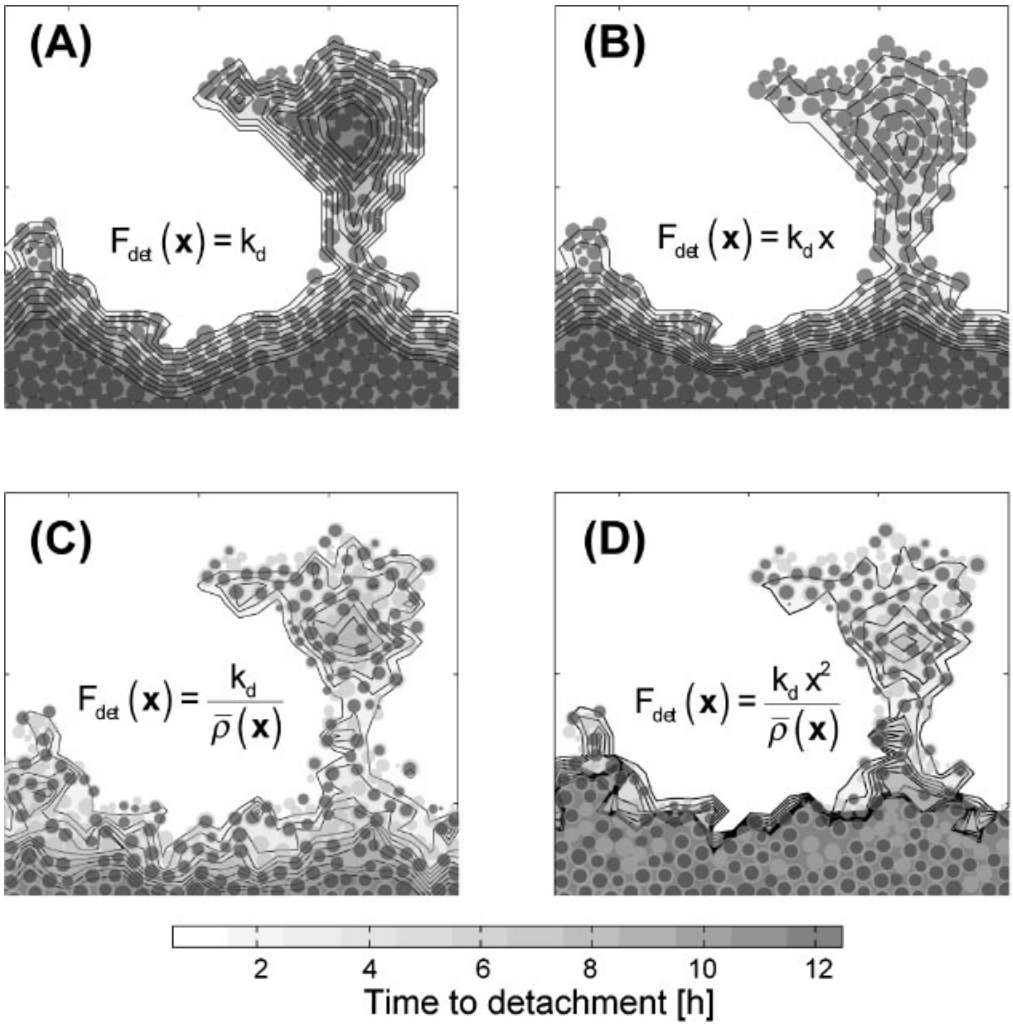

Figure 2. Four examples of $T(\mathbf{x})$ fields resulted from solving Equation 4 with different detachment speed functions F_{det}. Isocontours of $T(\mathbf{x})$ are displayed both with black curves and with grey shades ranging from white meaning imminent detachment to dark grey being areas detachable at later times. The simulated biofilm structure is derived from individual based modelling, where biomass is represented discretely by hard round particles. Four examples of detachment speed functions are shown: (**A**)—constant F_{det}. Local detachment rates are uniquely a function of the surface curvature, being higher in outward features of the surface and lower in the interior of concave features. This can be observed in the isocontours of $T(\mathbf{x})$ values shown, in which lines spaced further apart represent local high detachment rates. (**B**)—local detachment rates are first order proportional to the distance to the surface (x), i.e. higher at the top. For cases where biomass density is variable in space, F_{det} may be a function of the local density, such as the examples in (**C**) and (**D**). In these examples, biomass particles are composed of two substances of different density: active mass (represented by the dark circles) and extracellular polymeric substances (EPS, represented by light grey circles) of lower density. When local detachment rates are set inversely proportional to the local biomass density, $\bar{\rho}(\mathbf{x})$, detachment rates will be higher where local concentrations of EPS (less dense) are higher.

the distance to the solid substrate was chosen because it ensures the existence of a steady-state (Stewart, 1993) even for the extreme case of unlimited growth, i.e. growth at $R_H = \mu^{max} C_H$ for the entire biofilm. Values for the parameters used in the model are listed in Table I. Simulations were carried out using the IbM approach presented in Xavier et al. (2005) including the detachment routines described above.

Simulation Results

Simulations were carried out in both 2D and 3D spaces. Five 2D simulations, each representing 1 year of biofilm growth, were carried out keeping all parameters constant with the exception of the detachment speed coefficient, k_{det}. 2D simulations were named IA (highest k_{det}) to IE (lowest k_{det}). k_{det} values used are shown in Table I. Videos of the simulations carried out are provided at our website: http://www.biofilms.bt.tudelft.nl/detachmentPaperMaterial/index.html

Figure 3 shows results for the simulations IA and IE, the highest and lowest detachment cases, respectively. Panels labelled (**A**) and (**G**) show the time course of the maximum biofilm thickness (black line) for simulations IA and IE, respectively. Maximum biofilm thickness, L_f, is the distance from the solid surface to the tallest biofilm feature. Also shown in the same plots is the equivalent thickness of biomass, λ_f (grey line). This value is the total volume occupied by the biofilm (excluding voids) divided by the area

Table I. Parameters used for model in case study I.

Parameters	Description	Value	Units	Notes/references
Solute species				
C_o^{bulk}	Bulk concentration	0.004	$gO\,L^{-1}$	
D_O	Diffusivity	2×10^{-4}	$m^2\,day^{-1}$	Rittmann et al. (2004)
Particulate species				
ρ_H	Biomass specific mass	200	$gCOD\text{-}H\,L^{-1}$ particle	
Yield Coefficients				
Y_{OH}	Yield of oxygen on produced biomass	0.505	gO/gCOD-H	Beun et al. (2002)
Processes				
μ^{max}	Maximum specific growth rate of micro-organisms	11.3	$gCOD\text{-}H/gCOD\text{-}H\ day^{-1}$	Beun et al. (2002)
K_O	Saturation constant	3.50×10^{-4}	$gO\,L^{-1}$	Rittmann et al. (2004)
Computation parameters				
System size 2D		4000×31	μm^2	For 2D simulations
System size 3D		500×500	μm^2	For 3D simulations
$R_{division}$	Maximum particle radius	6	μm	
L_{bl}	Boundary layer thickness	200	μm	
Δx	Grid element size	30	μm	For 2D simulations
Detachment speed constants used in simulations				
k_{det}	Simulation IA	0.95	$m^{-1} \cdot h^{-1}$	
k_{det}	Simulation IB	3.2	$m^{-1} \cdot h^{-1}$	
k_{det}	Simulation IC	9.5	$m^{-1} \cdot h^{-1}$	
k_{det}	Simulation ID	31.7	$m^{-1} \cdot h^{-1}$	
k_{det}	Simulation IE	95	$m^{-1} \cdot h^{-1}$	

of the solid surface and has units of length. Together, L_f and λ_f define the value of the biofilm porosity, ε (not shown in Fig. 3), through the following relation

$$\varepsilon = 1 - \frac{L_f}{\lambda_f} \quad \text{[dimensionless]} \tag{9}$$

In panels (**A**) and (**G**), differences between the values of L_f and λ_f indicate formation of porous biofilms. Panels (**B**) and (**H**) show the time course of the total biomass detachment rate (R_{det}, biomass detached by both erosion and sloughing, black line) and the erosion rate only (R_{ero}, grey line). Differences between the two lines indicate the occurrence of sloughing events. These are especially visible for simulation IE (panel (**H**)), where peaks on the black line represent a sloughing event each. Panels (**C**) to (**F**), referring to simulation IA, and panels (**I**) to (**L**), referring to simulation IE, show biofilm structures at different times in the simulation together with the spatial concentration of dissolved oxygen at that time. For each of the 2D structures shown, vertical profiles of biofilm areal porosity, ε_A, and of the average concentration of oxygen are also shown in a separate plot on the left-hand side of each panel. Areal porosity, a parameter commonly used to characterise the distribution of biomass in biofilm (Lewandowski et al., 2004; Yang et al., 2000), is defined as the ratio of void area to the total area at each distance from the solid substratum. ε_A is related to the total biofilm porosity, ε, since the latter is the value ε_A averaged throughout the entire biofilm thickness.

Figure 4 shows the trends for the steady-state properties of the biofilm obtained from the five 2D simulations. The index *ss* will be used to indicate that a biofilm property is averaged in time over a defined steady state period, of duration Δt_{SS}. For example $L_{f,ss}$ refers to the maximum biofilm thickness in steady state and is obtained from

$$L_{f,ss} = \frac{1}{\Delta t_{ss}} \int_{\Delta t_{ss}} L_f \, dt \quad \text{[L]} \tag{10}$$

Panel (**A**) shows the value of the biofilm thickness, $L_{f,ss}$, for each simulation. Error bars represent the maximum fluctuation of L_f in the steady state period. Pane (**B**) shows the steady state porosity, ε_{SS}, versus the value of $L_{f,ss}$ for each simulation. Panes (**C**) and (**D**) show the steady state rates of produced biomass ($R_{H,ss}$) and detachment ($R_{det,ss}$ total, $R_{ero,ss}$ erosion and $R_{slo,ss}$ sloughing rates, respectively).

Figure 5 shows the size distribution of particles detached by sloughing in the course of the 2D simulations. The equivalent diameter of particles, ϕ_{eq}, is here used to quantify particle size. This value corresponds to the diameter of a round particle with the same volume as the irregularly-shaped detached particle. A minimum size for sloughing was arbitrary set at 50 μm, meaning only detachment of particles greater than 50 μm is considered a sloughing event. Particles with smaller ϕ_{eq} where classified as being part of the eroded material.

Biofilm Development in High Erosion Regime (Simulation IA)

In simulation IA, the biofilm thickness, L_f, reached the value of 114 μm early in the simulation, on day 20 (see Fig. 3A).

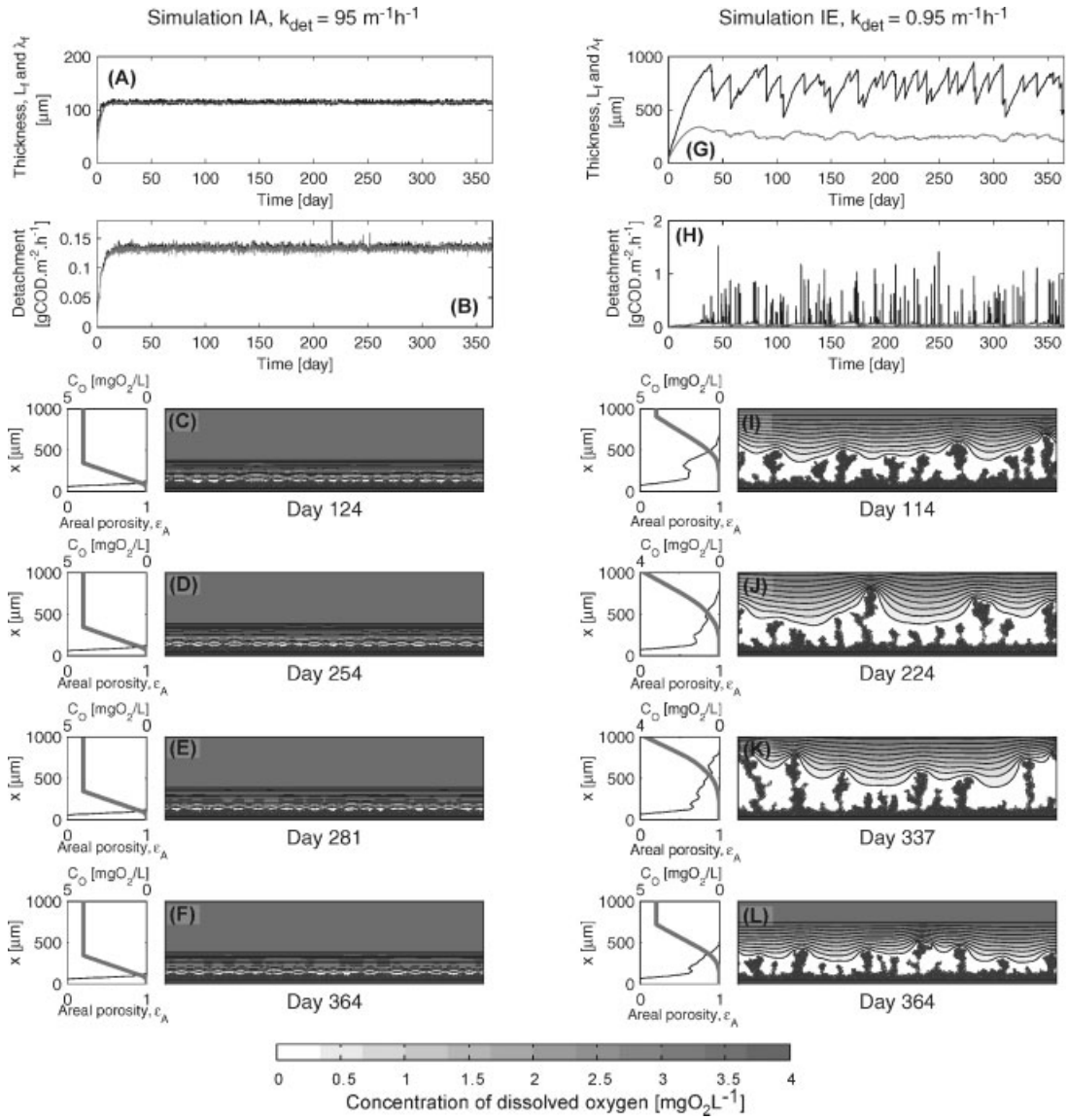

Figure 3. Results from 2D simulations of the system presented in case study I, for the simulations IA (run at the highest k_{det} of 95 $m^{-1} \cdot h^{-1}$) and IE (run at the lowest k_{det} of 0.95 $m^{-1} \cdot h^{-1}$). (**A**) and (**G**)—time course of maximum biofilm thickness, L_f (black lines), and equivalent biofilm thickness, λ_f (grey lines). (**B**) and (**H**)—time course of biomass detachment rate discriminated by total detached biomass (R_{det}, black lines) and biomass detached by erosion only (R_{ero}, grey lines). (**C**), (**D**), (**E**) and (**F**)—simulated biofilm structure at 124, 254, 281 and 364 days for simulation IA. (**I**), (**J**), (**K**) and (**L**)—simulated biofilm structure at 114, 224, 337 and 364 days for simulation IE. For the biofilm structure panes (C to F and I to L) the plot on the right hand side shows the vertical distribution of biofilm areal porosity (black thin line) and of avege oxygen concentration (gray thick line) at that time. Spatial concentrations of dissolved oxygen are shown as a colour iso-concentration plots in the background of the biofilm structure (right-hand side plots in these panes). Color legend for spatial concentrations of dissolved oxygen is shown at the bottom of the figure.

From that time until the end of the simulation, the value of L_f varied within a very narrow 12 µm range. Other biofilm properties (porosity, oxygen consumption rate and detachment rate) became practically constant from day 20 and, therefore, it was concluded that the biofilm had reached a steady state. The biofilm in the steady state had a very low porosity, as observed from the values of L_f and λ_f showing practically the same values (see Fig. 3A). Biomass detachment was characterised by the absence of sloughing events, which is observed from Figure 3B showing that total detachment (black line) was entirely due to erosion (grey line). The morphology observed from the pictures (Fig. 3C, D, E and F), showed a thin and smooth biofilm with very little variability in time.

Biofilm Development in Low Erosion Regime (Simulation IE)

In simulation IE, biofilm thickness (Fig. 3G) never reaches a value constant in time. Apart from the initial development period of 40 days, the value of L_f shows wide fluctuations ranging from 430 to 950 µm. After day 40, the biofilm was very porous throughout the simulation. This is observable from the difference between L_f and λ_f shown in Figure 3G,

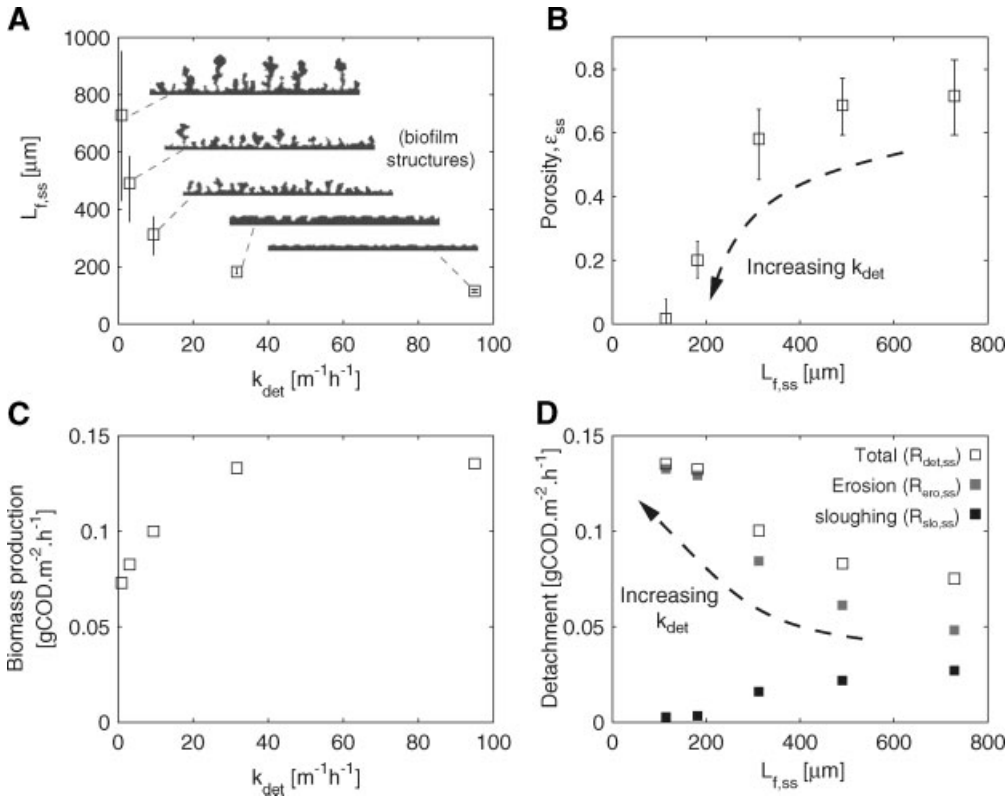

Figure 4. Results for case study I: Trends in steady state activity and structure of a biofilm grown at different detachment conditions from 2D simulations. (**A**)—steady-state biofilm thickness, $L_{f,ss}$. Error bars show the range between maximum and minimum value of L_f observed in the course of the steady state period. Typical steady state biofilm structures are also shown. (**B**)—steady state biofilm porosity, ε_{ss}, versus $L_{f,ss}$. (**C**)—steady state rate of biomass production. (**D**)—steady state detachment rate showing total detachment (R_{det}, empty squares), erosion (R_{ero}, grey squares) and sloughing (R_{slo}, empty squares) versus $L_{f,ss}$.

but is also visible from the biofilm structures shown in Figure 3I, J, K and L. The time course of R_{det} and R_{ero} (Fig. 3H) indicates the frequent occurrence of sloughing events throughout the simulation (sloughing events are shown by a peak in the value of R_{det}, the black line). The fluctuations in the value of L_f observed in Figure 3B are explained from these sloughing events, which occurred apparently at arbitrary times when tall finger-like structures rising from the biofilm (as seen in Fig. 3I, J, K and L) detach by erosion of its base. These finger like structures reach sizes big enough that growth at their base becomes oxygen limited, as seen previously for unrestricted biofilm growth (Picioreanu et al., 1998). The base, where biomass growth is slow but erosion forces are still significant, eventually detaches completely, causing the sloughing of the entire finger-like structure. In spite of these fluctuations in biofilm thickness and other biofilm properties, a ''noisy'' steady state was still observed. ''Noisy'' steady states are characterised by biofilm quantity and activity that are constant in the long term, in spite of arbitrary short-term fluctuations, and are typical of systems where sloughing events are significant (Morgenroth and Wilderer, 2000). The total biomass accumulation in the period ranging from day 30 to the end of simulation, at day 365, shows a value of 1.1×10^{-3} $\mathrm{gCOD \cdot m^{-2} \cdot h^{-1}}$, lower than that observed for simulation IA (1.5×10^{-3} $\mathrm{gCOD \cdot m^{-2} \cdot h^{-1}}$) for which the steady state was more evident (see biofilm accumulation rates for simulations IA to IE in Table II). To assess if the steady-state values are reproducible, an additional set of five replicate simulations at $k_{det} = 9.5$ $\mathrm{m^{-1}\,h^{-1}}$, initiated using different seeds of the random number generator, was carried out. From the results of those simulations it was concluded that the ''noisy'' steady state is computationally reproducible (Xavier et al., 2004).

Overall Trends in Biofilm Structure and Activity

Comparing the data from simulation IA (highest k_{det} case) and simulation IE (lowest k_{det} case) reveals that the formation of finger-like biofilm structures induced by oxygen concentration gradients is not possible if erosion forces present are very high. When detachment is low and finger-like structures are indeed formed, sloughing events cause fluctuations in the biofilm structural parameters, resulting in a ''noisy'' steady state. Figure 4 compares steady-state results for the five simulations carried out (simulations IA to IE). The steady state thickness, $L_{f,ss}$, (Fig. 4A) and the porosity (Fig. 4B) decreased with increasing k_{det}. When k_{det} was lower, biofilm thickness was highly variable in time (observable from the error bars shown) reflecting the fluctuations in the biofilm thickness caused by sloughing events. These differences in morphology had consequences in the biofilm activity, here defined in terms of the rate of biomass production (R_H, shown in Fig. 4C). R_H is lower when k_{det} is lower, in spite of all other parameters remaining constant. This decrease in biofilm

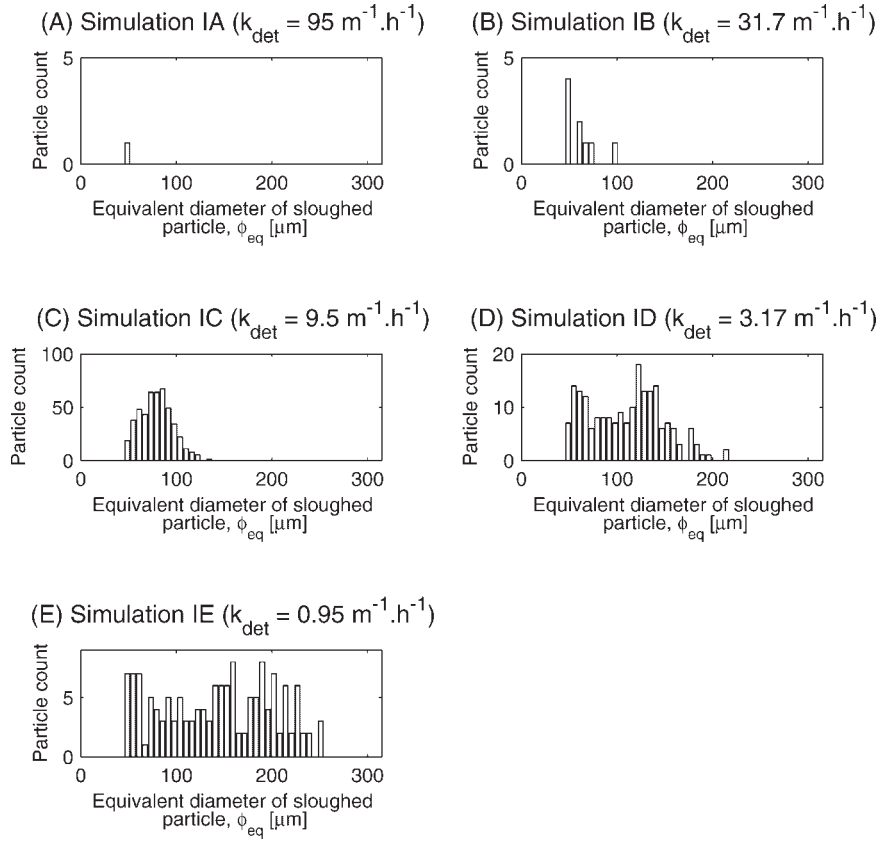

Figure 5. Size of sloughed particles for 2D simulations carried out in case study I, showing number of particles detached by sloughing distributing according to the value of their equivalent diameter (ϕ_{eq}). $k_{det} = 95\ m^{-1} \cdot h^{-1}$ (**A**), $k_{det} = 31.7\ m^{-1} \cdot h^{-1}$ (**B**), $k_{det} = 9.5\ m^{-1} \cdot h^{-1}$ (**C**), $k_{det} = 3.17\ m^{-1} \cdot h^{-1}$ (**D**) and $k_{det} = 0.95\ m^{-1} \cdot h^{-1}$ (**E**). Size distribution is shown for sloughed particles with equivalent diameter greater than 50 μm.

activity was a consequence of the irregular surface shape of the biofilm, which increased the mass transfer resistance to the biofilm as reported previously from both experimental (Wasche et al., 2000) and from modelling studies (Eberl et al., 2000; Picioreanu et al., 2000b). The observed trend in the end is that increasing the imposed detachment stress results in an increase in the activity of the biofilm.

From Figure 4D, it is observable that the sloughing rate was decreased with increasing erosion forces applied, in spite of the general trend that total detachment rate (R_{det}) increased. This result is in agreement with experimental observations that in biofilm airlift suspension (BAS) reactors imposing stronger detachment has as consequence a reduction in sloughing (Van Loosdrecht et al., 1995). The size distribution of sloughed particles (shown in Fig. 5) illustrates that the range of sizes of particles sloughed increased with decreasing detachment forces. At high detachment (simulations IA shown in Fig. 5A, IB shown in Fig. 5B and IC shown in Fig. 5C), only particles smaller than 100 μm detached. In simulation IE (lowest k_{det}), however particles up to 250 μm were observed. This indicates that not only the total rate of sloughing is higher when imposed erosion forces are lower, but also that the particles detaching will be bigger. A different trend is observed for the total number of particles detached by sloughing. Figure 5C representing simulation IC (corresponding to the simulation carried out with the middle-range value k_{det} of 9.5 $m^{-1} \cdot h^{-1}$) shows the highest number of particles sloughed in the course of the simulation (5,935 sloughed particles). In this simulation, a large number of small size particles detached by sloughing. However, the highest number of sloughed particles does not correspond to the highest rate of sloughing in terms of total biomass loss by sloughing, as shown in Figure 4D (sloughing rate shown in black squares).

Simulations were also carried out in 3D. Figure 6 shows examples of 3D structures obtained from simulations carried

Table II. Biofilm average biomass production, biomass detachment and biomass accumulation (production-detachment) rates in the 30–365 days period. Biomass production and biomass losses through detachment have very similar average values in this time period, which results in very low biomass accumulation rates. Hence, the biofilm is in steady state, even for simulations were fluctuations in biofilm thickness in the course of the simulation are high.

Simulation	Average biomass production [$gCOD \cdot m^{-2} \cdot h^{-1}$]	Average biomass detachment [$gCOD \cdot m^{-2} \cdot h^{-1}$]	Average biomass accumulation [$gCOD \cdot m^{-2} \cdot h^{-1}$]
IA	0.135	0.134	0.002
IB	0.133	0.129	0.003
IC	0.100	0.098	0.002
ID	0.082	0.081	0.001
IE	0.073	0.072	0.001

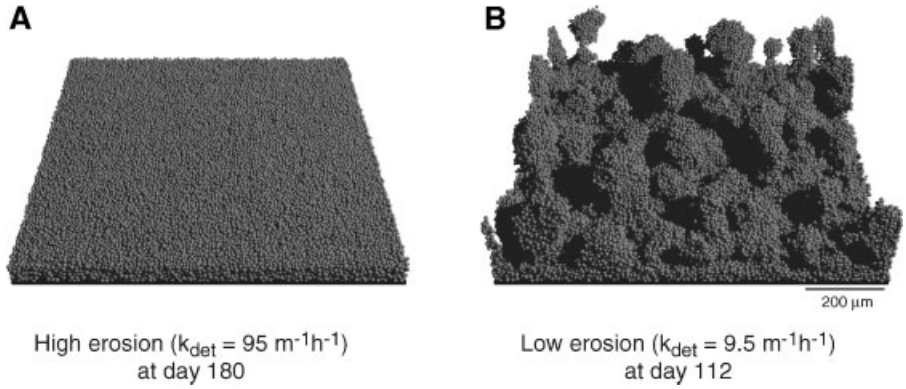

Figure 6. Structures obtained from 3D simulations of biofilm grown at (**A**) high (smooth structure) and (**B**) low (heterogeneous structure) k_{det} values. The 3D structure shown for the low detachment case is representative of the ''dynamic steady state'' observed,, i.e. short term changes in the structure occur as a result of sloughing events but long term biofilm features are maintained in the long term.

out with different values of k_{det}. See also the web site referred above for animations of the 3D simulations. Results from 3D simulations showed the same trends for steady state biofilm activity and structure described for 2D, further supporting our opinion that 2D studies are sufficient for the analysis of trends from multidimensional biofilm modelling (Eberl et al., 2000). 2D studies are usually preferable to studies in 3D as, for the latter, simulations are significantly more demanding computationally.

CASE STUDY II: INFLUENCE OF DETACHMENT ON BIOFILM DENSITY

Heterogeneity in biofilm structure is also manifested in the spatial distribution of biomass components in the biofilm matrix. The present case study uses a representation of biomass that discriminates between active mass, inert biomass and extracellular polymeric substances (EPS). In contrast to approaches where biomass composition is assumed to be homogeneous, as in case study I, structured representations of biomass allow a description of spatial variation of biofilm density. Biomass losses by processes of EPS hydrolysis and decay of heterotrophic biomass and the recycling of substrate originating from these processes into biomass growth are also considered here.

Representations of structured biomass with EPS, active heterotrophic mass and inert mass has been reported for the 1D modelling of biofilm development in a tube reactor (Horn et al., 2001) and 2D cellular automata simulations of biofilm development (Laspidou and Rittmann, 2004). Both these reports described the use of the products of EPS degradation as carbon and energy source for microbial growth, which is supported by experimental observations (Zhang and Bishop, 2003). The present case study will demonstrate how the detachment methodology used here may be used to study the dynamics of biofilm structure in long term simulations, up to 100 days of biofilm growth. The kinetic model presented here derives from a simplification of the models presented in the above-mentioned studies.

Model Description

Biomass is composed of three particulate components: heterotrophic active mass (H), extracellular polymeric substances (EPS) and inert mass (I). A soluble substrate (S) used as carbon and energy source by the bacteria and oxygen (O) are the only two rate limiting soluble species considered in the system. The model system considers three reactions: substrate uptake for heterotrophic growth, decay of heterotrophic bacteria and hydrolysis of EPS. EPS production is coupled to biomass growth, both defined in terms of yields of the rate of substrate uptake. Rates and yields for these reactions are shown in Table III. The values for the parameters used in the simulations are presented in Table IV.

Table III. Process matrix used in case study II. Rows in the matrix represent the reactions occurring and columns represent the species (solute and particulate) in the system. Entries in the matrix are the yield coefficients, with empty entries effectively representing the value 0. The last column shows the expression for the reaction rate. $\varphi_{M,S}$ and $\varphi_{M,O}$ represent Monod factors of substrate and oxygen concentrations respectively.

	Solute species		Particulate species			
Reaction	Substrate (C_S)	Oxygen (C_O)	Active mass (C_H)	EPS (C_{EPS})	Inert (C_I)	Rate
Substrate uptake by heterotrophic bacteria	−1	$-(1-Y_{SH}-Y_{SEPS})$	Y_{SH}	Y_{SEPS}		$q_S^{max} \cdot \varphi_{M,S} \cdot \varphi_{M,O} \cdot C_H$
Decay of heterotrophic bacteria	0.6		−1		0.4	$B_{decay} \cdot C_H$
Hydrolysis of EPS	1			−1		$k_{hyd} \cdot C_{EPS}$

Where $\varphi_{M,S} = \frac{C_S}{C_S+K_S}$; $\varphi_{M,O} = \frac{C_O}{C_O+K_O}$.

Table IV. Parameters used for model in case study II.

Parameters	Description	Value	Units	Notes/references
Solute species				
C_o^{bulk}	Bulk concentration of oxygen	0.004	$gO_2\,L^{-1}$	
D_O	Diffusivity of oxygen	2×10^{-4}	$m^2\,day^{-1}$	Rittmann et al. (2004)
D_S	Diffusivity of substrate	1×10^{-4}	$m^2\,day^{-1}$	Rittmann et al. (2004)
Particulate species properties				
ρ_H	Specific mass of biomass	200	gCOD-H L^{-1} particle	
ρ_{EPS}	Specific mass of EPS	33.3	gCOD-EPS L^{-1} particle	6 times less dense than active biomass (Horn et al., 2001)
ρ_I	Specific mass of inert biomass	200	gCOD-I L^{-1} particle	Equal to density of active biomass (Horn et al., 2001)
Yield coefficients				
$Y_{SH} + Y_{SEPS}$	Yield of total biomass on substrate	0.495	gCOD-H/gCOD-S	Beun et al. (2002)
Y_{SH}	Yield of biomass on substrate	0.20625	gCOD-H/gCOD-S	Derived from ratio obtained from (Horn et al., 2001)
Y_{SP}	Yield of polymers on substrate	0.28875	gCOD-EPS/gCOD-S	Derived from ratio obtained from (Horn et al., 2001)
Rate parameters				
q_S^{max}	Maximum substrate uptake rate of micro-organisms	0.952	gCOD-S/gCOD-X h^{-1}	Beun et al. (2002)
b_{decay}	Decay rate	3.3×10^{-3}	gCOD-X/gCOD-X h^{-1}	Rittmann et al. (2004)
k_{hyd}	EPS hydrolysis rate coefficient	0.014	gCOD-EPS/gCOD-EPS h^{-1}	Horn et al. (2001)
K_S	Saturation constant for substrate	0.004	gCOD-S L^{-1}	Rittmann et al. (2004)
K_O	Saturation constant for oxygen	3.50×10^{-4}	$gO_2\,L^{-1}$	Rittmann et al. (2004)
Computational parameters				
System size		2000×2000	μm^2	
$R_{division}$	Maximum particle radius	8	μm	
R_{min}	Minimum particle radius	0.1	μm	
L_C	Boundary layer thickness	100	μm	
Δx	Grid element size	30.3	μm	
k_{det}	Detachment speed constant	3×10^{-3}	gCOD $L^{-1}\,\mu m^{-1}\,h^{-1}$	
Bulk substrate concentrations used in simulations				
C_S^{bulk}	Simulation IIA	0.1	gCOD-S L^{-1}	
C_S^{bulk}	Simulation IIB	0.02	gCOD-S L^{-1}	
C_S^{bulk}	Simulation IIC	0.008	gCOD-S L^{-1}	
C_S^{bulk}	Simulation IID	0.004	gCOD-S L^{-1}	
C_S^{bulk}	Simulation IIE	0.0015	gCOD-S L^{-1}	
C_S^{bulk}	Simulation IIF	0.0008	gCOD-S L^{-1}	

As shown in Table III, the rate of substrate uptake by microorganisms is a function with dual limitation by the concentrations of substrate and oxygen. The biomass growth as defined here can be either substrate-limited or oxygen-limited, depending on the bulk concentrations of substrate, C_S^{bulk}. The bulk concentration of oxygen is kept constant for all simulations. If the concentration of substrate is high, sharp gradients of oxygen will arise as soon as the biofilm thickness becomes large enough, with low oxygen concentrations next to the solid substratum. In such cases, growth becomes oxygen-limited. In contrast, if the substrate concentration is low, substrate concentration will be the growth-limiting factor. In order to quantify the growth regime as either oxygen-limited or substrate-limited, the penetration depth, *PD*, of a solute species is used. *PD* is here defined for a generic solute species i as the distance from the biofilm top (located at distance L_f from the solid surface) at which mean solute concentration reaches a value lower than 10% of the half-saturation constant for that solute, K_i.

Biomass detachment is in this case modelled using a detachment speed function that is a second order function dependency of the distance to the solid substratum, x, but also a function of the local biofilm density ρ, as follows

$$F_{det}(\mathbf{x}) = \frac{k_{det} x^2}{\rho(\mathbf{x})} \quad [LT^{-1}] \tag{11}$$

with k_{det} having dimensions of $M \cdot L^{-4} \cdot T^{-1}$. This expression causes lower detachment rates where local values of the biofilm density are higher. This feature reflects observations that increased biofilm density is associated with a higher resistance to detachment forces (Kwok et al., 1998; Van Loosdrecht et al., 1995).

The model was implemented using the same IbM as for case study I (Xavier et al., 2005). EPS production by microorganisms was integrated in the procedure as described previously (Kreft and Wimpenny, 2001). Following that approach, EPS produced is represented as a particle sur-

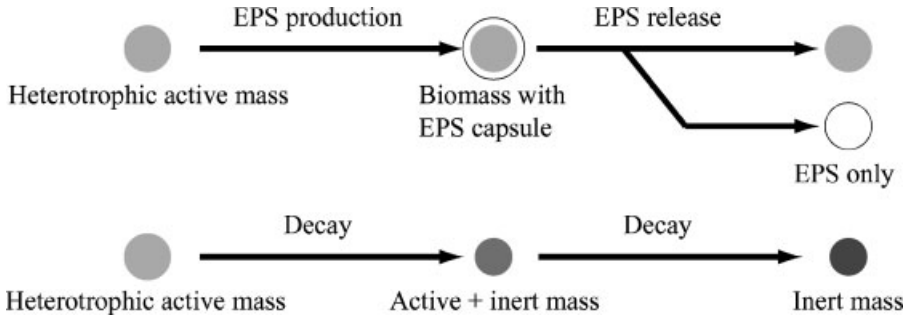

Figure 7. Illustration of the particle based modelling of biomass extended with EPS production and biomass decay used in case study II. Colour code used represents the biomass composition: EPS is represented as a white capsule surrounding the remaining biomass constituents. Biomass particles are represented by a shade of grey representative of their composition in heterotrophic active mass and inert biomass. Darker tones represent a higher fraction of inert mass in the biomass.

rounding the remaining biomass components. EPS-only biomass particles are generated by EPS excretion as illustrated in Figure 7.

Simulation Results

Six simulations with the bulk concentration of substrate, C_S^{bulk}, ranging from 0.1 to 0.0008 gCOD-S L^{-1} (values of remaining parameters are in Table IV) were carried out in 2D following 100 days of biofilm development. Simulations for case study II will be here referred using nomenclature IIA (highest C_S^{bulk}) to IIF (lowest C_S^{bulk}). Videos of the simulations carried out are provided at our website: http://www.biofilms.bt.tudelft.nl/detachmentPaperMaterial/index.html

Figure 8 shows selected simulation results distributed in three columns of panels: IIA in column (A), IIC in column (B) and IID in column (C). The first line shows maximum biofilm thickness, L_f (black line), and the equivalent

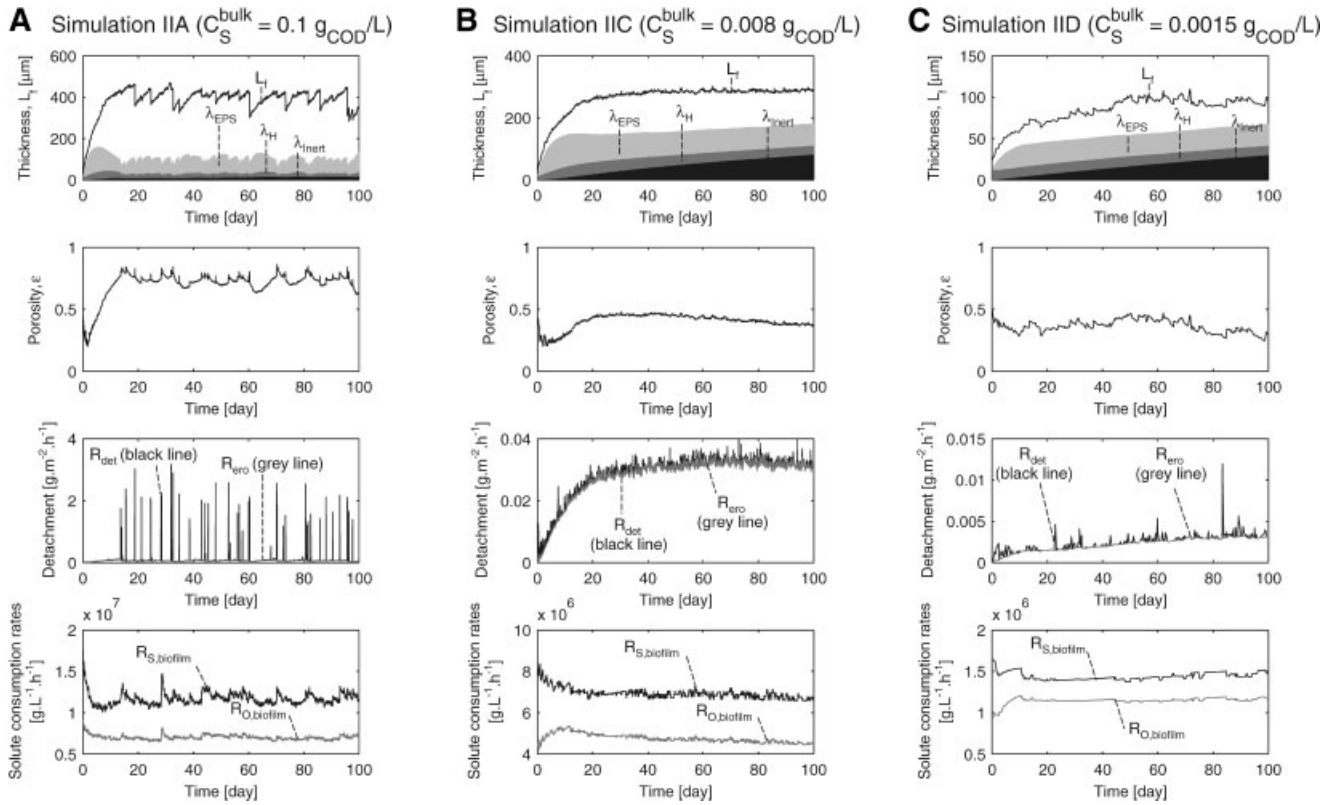

Figure 8. Time course of biofilm properties for simulations IIA shown in column of panels (**A**), IIC shown in column (**B**) and IIC shown in column (**C**). The first line of panels shows maximum biofilm thickness, L_f (black line), and the equivalent thickness of the biomass components represented by area plots: λ_{EPS} (EPS, shown in light grey), λ_H (active mass, shown in dark grey) and λ_{Inert} (inert mass, shown in black). The second line of panels shows the time course of the biofilm porosity, as defined in Equation 9. The third line shows the time course of the detachment rates, picturing the total detachment rate (R_{det}, black line) and the rate of detachment via erosion (R_{ero}, grey line). Differences between the two lines represent the occurrence of sloughing events. The last line of panels shows the net consumption rates for the solute species, oxygen ($R_{O,biofilm}$) and substrate ($R_{S,biofilm}$), in the biofilm.

thickness of the biomass components represented by area plots: λ_{EPS} (EPS, shown in light grey), λ_H (active mass, shown in dark grey) and λ_{Inert} (inert mass, shown in black). The equivalent thickness of a biofilm component, termed λ_i for a generic particulate species i in the biofilm, is here defined by

$$\lambda_i = \frac{\sum_{j=1}^{N_{particles}} M_{i,j}}{\rho_i} \cdot \frac{1}{L_y L_z} \quad [\mathrm{L}] \tag{12}$$

The remaining data shown concerns the time course of biofilm porosity (ε), detachment rates (R_{det}, R_{ero} and R_{slo}) and the total net consumption rates for the solute species, oxygen ($R_{O,biofilm}$) and substrate ($R_{S,biofilm}$), in the biofilm.

Figure 9 displays biofilm structures at a representative time for simulations IIA, IIC and IID, with each line of panes representing a time point in simulation. Figure 10 presents the overall trends observed from results of simulations IIA through to IIF. Values shown here are average values of biofilm properties in the period from day 20 until the end of the simulation at day 100. The period following the initial development of 20 days is here called the ''mature state'' period of the biofilm. The term mature state is used here instead of steady state, since no real steady state of biofilm composition was detected, as will be discussed later. The index *ms* will be used to indicate that a biofilm property is averaged over the mature state. For example $L_{f,ms}$ shown in panel (**A**) of this figure refers to the maximum biofilm thickness time average in the period from day 20 to day 100, as follows

$$L_{f,ms} = \frac{1}{80}\int_{\text{day 20}}^{\text{day 100}} L_f \, dt \quad [\mathrm{L}] \tag{13}$$

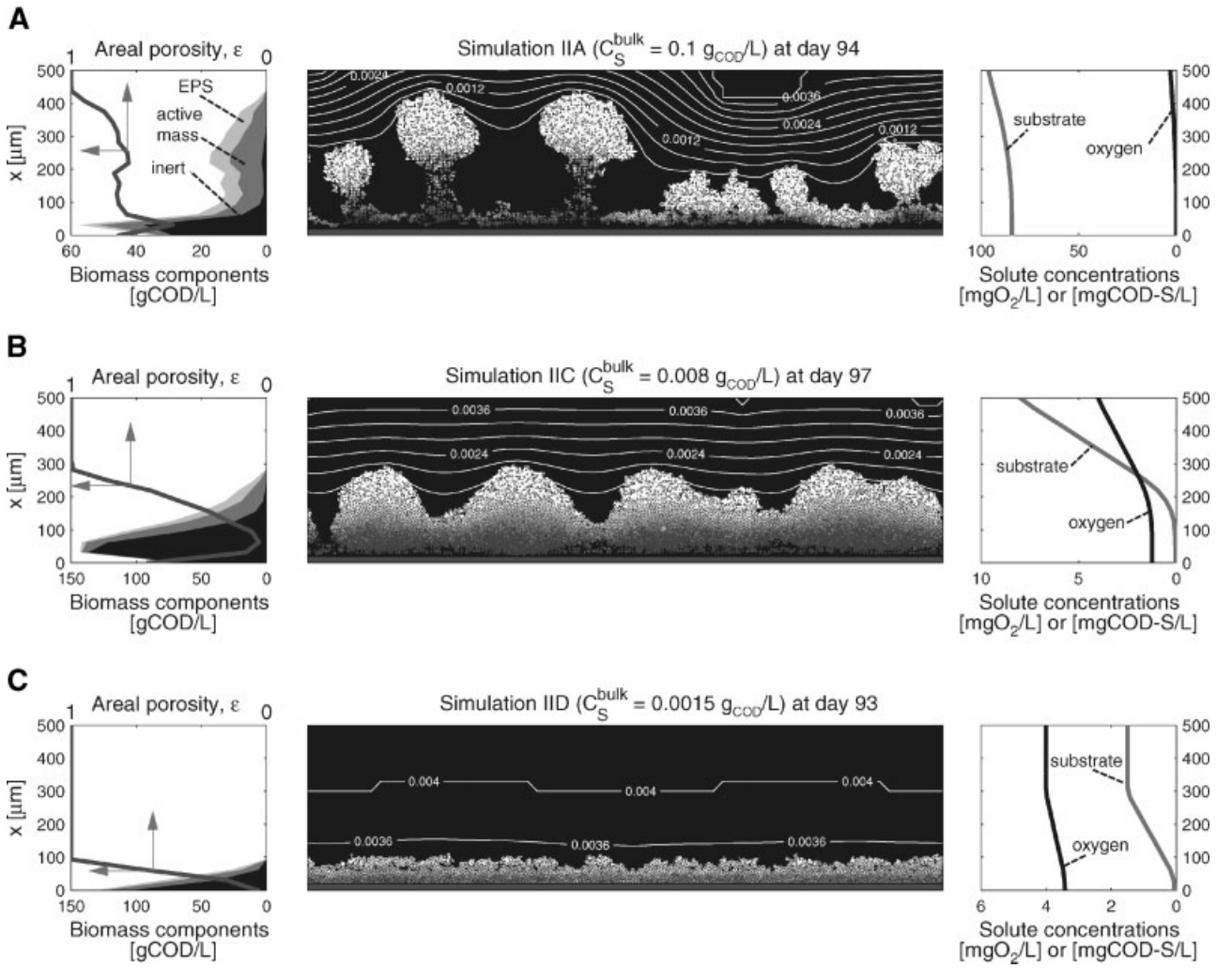

Figure 9. Biofilm structure at representative time points in simulations. (**A**) day 94 of simulation IIA. (**B**) day 97 of simulation IIC. (**C**) day 93 of simulation IID. Panels in the first column show profiles of the biomass properties along the biofilm depth, namely the areal porosity, ε_A (dark gray line), and the average mass of biomass components (area plots with EPS in light grey, active mass in dark grey and inert mass in black). The second column shows the biofilm structure with the color of each biomass particle representing its composition in EPS, active mass and inert, as illustrated in Figure 7. Iso-concentration lines of dissolved oxygen concentration are also shown. The last column shows the profiles of average concentration of solutes, oxygen (black line) and substrate (grey line), along the biofilm depth.

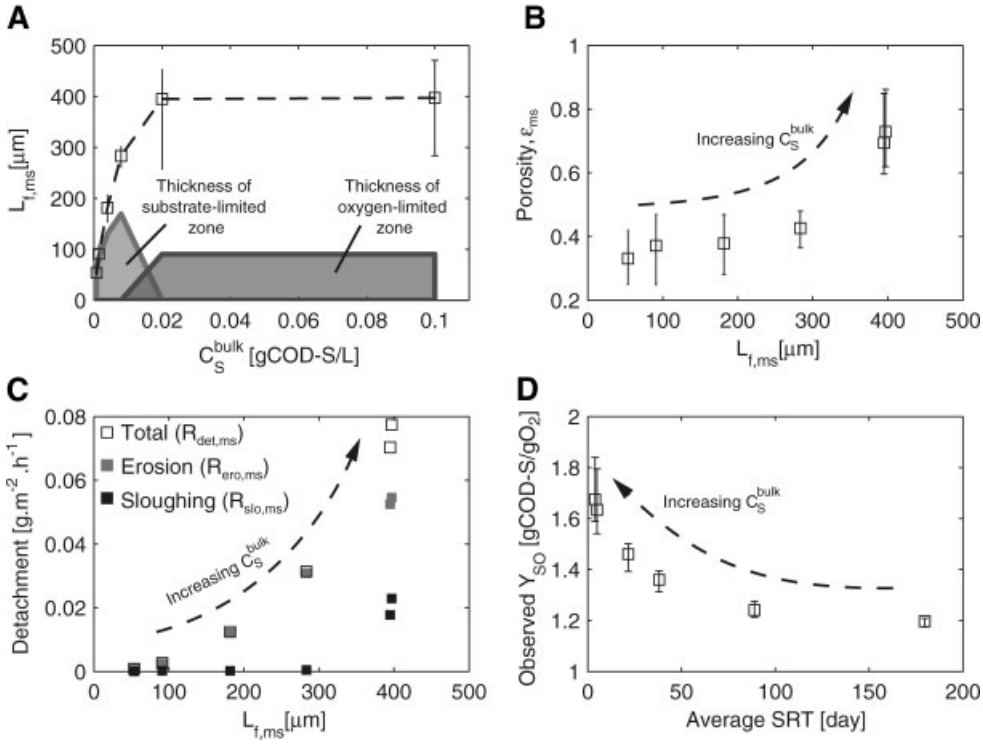

Figure 10. Trends in biofilm properties for the simulations carried out in case study II. (**A**) shows the average biofilm thickness ($L_{f,ms}$, shown as empty squares), with error bars representing here the range in the value of L_f observed in the 20–100 day period. (**B**) shows the value of the average biofilm porosity, ε_{ms}, versus $L_{f,ms}$. (**C**) shows the detachment rate averaged in time for the 20–100 day period versus $L_{f,ms}$. Detachment data is discriminated by total detachment ($R_{det,ms}$), erosion ($R_{ero,ms}$) and sloughing ($R_{slo,ms}$) rates. (**D**) shows the observed yield of consumed substrate per oxygen consumed in the biofilm (*observed* Y_{SO}) versus the average solids retention time (*SRT*).

Also presented in this plot is the thickness of the oxygen-limited, L_{ol}, and substrate-limited, L_{Sl}, zones. These data, represented as area plots is obtained from

$$L_\alpha = L_{f,ms} - PD_O \quad [\mathrm{L}] \tag{14}$$

$$L_{Sl} = L_{f,ms} - PD_S \quad [\mathrm{L}] \tag{15}$$

The *observed* Y_{SO} shown in panel (**D**) is here defined as the time average of the ratio between the net substrate consumption rate ($R_{S,biofilm}$) and net oxygen consumption rate ($R_{O,biofilm}$) in the biofilm, as described by

$$\text{observed } Y_{SO} = \frac{1}{80}\int_{20}^{100} \frac{R_{S,biofilm}}{R_{O,biofilm}}\,dt \quad [\mathrm{M_S \cdot M_O^{-1}}] \tag{16}$$

The average solids retention time in the biofilm is, here, the time average of the ratio between total biomass in the biofilm (M_f) and the detachment rate (R_{det}), as described by

$$\text{average } SRT = \frac{1}{80}\int_{20}^{100} \frac{M_f}{R_{\mathrm{det}}}\,dt \quad [\mathrm{T}] \tag{17}$$

Biofilm Growth in Oxygen-Limited Regime (Simulations IIA and IIB)

The biofilm in the two simulations carried out with higher bulk substrate concentration (IIA and IIB) reached a mature state after an initial development phase of 20 days (as shown for simulation IIA in Fig. 8A). From day 20, biofilm dynamics was characterised by fluctuations in the biofilm properties, similar to the ''noisy'' steady states reported in case study I. Biofilm thickness reached mean steady state values around 400 μm for both simulations IIA and IIB (see Fig. 10A), with fluctuations between 280 and 470 μm due to sloughing events. Substrate uptake rate was not substrate limited and sharp gradients in the oxygen concentration gradients were formed, as seen in Figure 9A. This induced the formation of finger-like biomass clusters that, by collapsing at the base, constituted the cause of sloughing events (as shown in the detachment rate pictured in Fig. 8A). The oxygen penetration depth, PD_O, reached values as low as 50% of the biofilm thickness, while the substrate completely penetrated the biofilm, confirming that growth was predominantly oxygen-limited for these two simulations. The biofilms formed were highly porous (shown in Fig. 10B) and with a high EPS content (20%–30% of the biomass). Areal porosity profiles revealed that the fraction of void spaces is higher in the outer regions of the biofilm and decreasing towards the solid surface (see Fig. 9A). A general trend occurring was the formation of a thin and porous attachment base and large tips full of EPS and active mass. Inert mass is found mainly in the interior of the biofilm, close to the solid substratum, where it is the major constituent (~75%) of the biomass. The fraction of inerts in the total biomass in the biofilm was observed to be considerably low in these two

simulations (ranging from 30% to 45%). A slight but steady increase in the fraction of inerts throughout the simulation was observed. The outer regions of the biofilm show very high fractions of active mass and EPS (Fig. 9A). The solids retention time (SRT) influences the effect of biomass decay. With longer SRTs the recycling of substrate released from decay processes (heterotrophic decay and EPS hydrolysis) will have a higher influence in the substrate turnover, as reflected by a higher *observed* Y_{SO} (shown in Fig. 10D) for IIA and IIB.

Biofilm Growth in Substrate-Limited Regime (Simulations IIC, IID, IIE and IIF)

Simulations carried out carried out at bulk substrate concentrations of 8×10^{-3} gCOD-S L^{-1} and lower (IIC, IID, IIE and IIF) equally showed an initial development phase of 20 days, in which biofilm thickness increased rapidly (Fig. 8B and C for simulations IIC and IID, respectively). Following this initial development stage, simulations IIC, IID, IIE and IIF showed a mature state that was significantly different to that observed from simulations IIA and IIB. From day 20 until the end of the simulation, all four simulations showed thinner biofilms (see Fig. 10A). In the course of this mature phase, biofilm activity (in terms of substrate and oxygen consumption) was kept practically constant for each simulation (seen in the bottom panes of Fig. 9B and C for simulations IIC and IID). The thickness of the oxygen limited zone was 0 at all times, while the thickness of the substrate limited zone (shown in Fig. 10A) increased with decreasing C_S^{bulk}. This indicates that the biofilms produced in simulations IIC, IID, IIE and IIF were predominantly substrate limited implying that maximum biomass growth rates were consequently lower than in simulations IIA and IIB. As a consequence, biofilms did not show the formation of tall finger-like biomass clusters, formation enhanced by faster growing biomass (Picioreanu et al., 1998). Instead, the biofilms formed ranged from thick wavy shapes (Fig. 10B, for simulation IIC), to thin biofilms (Fig. 9C, for simulation IID). Due to the absence of tall finger-like biomass clusters, biomass sloughing was practically non-existent for these simulations and most detachment occurred by erosion, as shown in Figure 10C. EPS content (10%–15% of the biomass) was also lower than in simulations IIA and IIB for all four simulations, with trends showing that more substrate originated more porous biofilms (see Fig. 10B) and with higher EPS content. Similar to simulations IIA and IIB, higher fractions of EPS and active mass formed in the outer regions of the biofilm, where substrate concentrations were higher (Fig. 9B and C, for simulations IIC and IID, respectively). Fractions of inert increased towards the interior of the biofilm. The fraction of total inert biomass in the biofilm was significantly higher than those observed for IIA and IIB, with trends showing higher inert fraction for simulations with the lowest bulk substrate concentration (up to 68% of the biomass at the end of simulation IIF). Values of observed Y_{SO} decreased from IIC ($Y_{SO}^{observed} =$ 1.39 gCOD-S/gO) to IIF ($Y_{SO}^{observed} = 1.17$ gCOD-S/gO), demonstrating that the effect of biomass decay is higher when bulk substrate concentrations are lower, and inversely proportional to the average SRT (shown in Fig. 10D).

Biomass Consolidation

For all four simulations IIC to IIF, a steady increase in inert biomass was observed throughout the simulations (first pane of Fig. 8B and C), however with different consequences. An effect that might be termed biomass consolidation was observed in the cases where C_S^{bulk} was higher. For example, in simulation IIC, the biofilm thickness (first panel of Fig. 8B) reached its mean mature state value of $L_{f,ms} = 280$ μm at day 30. At this time, the biomass distribution was (i) porous and with high EPS content at the top of the biofilm (150–280 μm), (ii) denser in an intermediate region (50–150 μm) and (iii) showing a large percentage of void spaces closest to the solid substratum. Deep biofilm biomass was composed mostly by inerts. For the remainder of the simulation, an increase in the quantity of inerts is observed (first panel of Fig. 8B), accompanied by a slight decrease in the active mass. It is observed that the total biomass in the biofilm increases, while the biofilm thickness remains constant. This was made possible by a reduction in the biofilm porosity (second panel of Fig. 8B). From areal porosity profiles, we observed that this reduction on porosity was localised mainly close to the solid substratum. Effectively, the increase in the inert content of the biofilm resulted in packing of the biomass in the depth, where inert mass produced in the upper and more active layers started filling the void spaces located below. A similar process of biomass consolidation was previously explicitly introduced as an assumption in the 2D CA model by Laspidou and Rittmann (2004). In the present study, however, biomass consolidation is as an emergent property of the biofilm growth simulation.

In simulations IIE and IIF practically no consolidation was observed, with the biofilm at day 20 already fully packed.

Trends Observed

In simulations IIA and IIB at higher substrate concentration growth was oxygen limited. In contrast, for simulations IIC to IIF carried out with lower substrate concentrations growth was substrate limited. The growth regime, whether oxygen or substrate limited, was found to be very significant in the biofilm development.

Simulations in oxygen-limited regime produced tall and highly porous biofilms and with a high EPS content. Sloughing events occurred frequently leading to a significant fraction of the total detached biomass (30% for simulation IIA and 25% for simulation IIB), as seen in Figure 10C. The fraction of inert biomass in the biofilm was low throughout the simulations, which is in agreement with the low average SRT values. Furthermore, values for the observed Y_{SO} revealed that the recycling of substrate originating from the decay of heterotrophic biomass and EPS hydrolysis was not very significant for growth.

Simulations in substrate limited regime, in turn, produced thin biofilms with low porosities, low EPS fractions and high content of inerts. No sloughing events were observed in these simulations and detachment occurred mainly by erosion. The fraction of inerts increased throughout all simulations, with biomass consolidation visibly occurring in simulations IIC and IID. The values of *observed* Y_{SO} were substantially lower than the value Y_{SO} of the reaction of substrate uptake, revealing the importance of substrate recycling in substrate limited growth conditions. This was also in agreement with the higher values of the average SRT: 22, 38, 89 and 180 days for simulations IIC, IID, IIE and IIF, respectively.

DISCUSSION AND CONCLUSIONS

The present study, together a previous study (Xavier et al., 2005), reports on a novel framework for the implementation of multidimensional biofilm models. The framework is based on well-established physical principles to describe the processes involved in biofilm formation and principles of mass conservation for the bioconversions occurring. The generic description of biomass detachment proposed here for multidimensional modelling of biofilms mimics important experimentally observed trends. While in reality detachment may occur from a variety of mechanisms, a distinction is made between those that act on the entire surface of the biofilm, such as erosion, and those which are localised both in time and space, i.e. sloughing events, but that still result from a combination of external forces and random instabilities in the structure (Morgenroth and Wilderer, 2000). The method described here uses Equation 1 to describe the first mechanism, and predicts the occurrence of the second from a combination with the heterogeneous biofilm structure. This is in accordance to the hypothesis that a distinction between sloughing and other detachment processes is arbitrary from a mechanistic point of view (Stewart, 1993). Results of the detachment model proposed here present the same behaviour as the more computational demanding mechanistic approach described in Picioreanu et al. (2001). The method described here can be used for both 2D and 3D simulations as shown in the first case study. Furthermore, although its integration with a model of biofilm growth was carried out with a framework that uses individual-based modelling, this methodology could similarly be integrated with other multidimensional biofilm approaches such as cellular automata or continuum models.

A simple model of biofilm growth was presented in case study I to illustrate how steady state biofilm structure and activity may be derived from simulations. The model showed that ranges in biofilm morphology and activity might be obtained by growing a biofilm under different erosion forces. For the simulations were erosion forces were lower, the biofilm reaches a quasi steady state, in which biomass detachment by sloughing is significant in balancing biofilm growth. The simulations shown here further illustrate the view that the relative importance of different detachment mechanisms occurring in biofilm reactors may change depending on the operating conditions (Morgenroth and Wilderer, 2000; Picioreanu et al., 2001).

Case study II that considers active mass, EPS and inerts, demonstrates the application of the detachment procedure in a case where the biomass composition is variable and the erosion speed is a function of the local biofilm density. Although both cases presented here are not multi-species biofilms, this methodology may be as well applied to multi-species systems. Such is the case of the system with two competing heterotrophic species, where the capability of one species to produce internal storage compounds is shown to play a selective advantage when feeding occurs in feast/famine cycles analysed elsewhere (Xavier et al., 2005).

These case studies are representative applications of a general-purpose framework for multidimensional biofilm modelling, which may be applied to describe a variety of bioconversion processes (Xavier et al., 2005). Although example applications have so far described systems where mass transport of solutes occurs by homogeneous diffusion, the framework provides the capability of using diffusion coefficients variable in space. This feature may be used to account for observed increased resistance to diffusion of solutes in the biomass matrix (Beuling et al., 2000; Bryers and Drummond, 1998). The detachment speed functions referred so far in the examples are a subset of the vast range of functions that may be used to describe various detachment scenarios. Possible future applications of this methodology may include detachment speed functions derived from models of fluid velocity and the effect of shear stress (Picioreanu et al., 2001), detachment as a function of the local concentration of specific compounds relevant to the integrity of the biofilm matrix, such as alginate in *Pseudomonas aeruginosa* biofilms (Boyd and Chakrabarty, 1994), or local concentrations of detachment inducing substances such as antimicrobial agents (Hunt et al., 2003).

It should be noted that the description of sloughing events provided in the method proposed here accounts for only a subset of possible types of sloughing events that may occur in a biofilm. Another possibility for sloughing events would be one resulting from loss of the adhesion between the biofilm matrix and the solid substrate, which would result in losses of larger amounts of biomass. It should equally be noted that the occurrence of tall finger like structures as the ones shown in Figures 3I and 9A is only possible in the cases when total bending forces acting on the biofilm structure are negligible in relation to the mechanical strength of the structures. This does not account for all practical cases, as fluid flow can often bend such structures into streamers.

A final note concerning a practical issue should be made in respect to the algorithm used for implementation of the detachment procedure. Solving Equation 4 using the fast marching level set, of key importance for this method, is an extremely fast and efficient operation. Thanks to this algorithm, the operations required to implement detachment have a low impact in the overall computation of a simulation cycle, as the time required is low in relation to other operations performed. This fact, added to the flexibility

permitted by the methodology and the other characteristics mentioned above, make this a method of choice for the description of detachment processes for multidimensional modelling of biofilms and an important tool for the study of biofilm dynamics.

NOMENCLATURE

Symbol	Definition	Dimensions
Γ	Surface of biofilm/liquid interface	$[L^2]$
Δt	Iteration time step	[T]
Δt_{SS}	Duration of a defined steady-state period	[T]
ΔV_i	Volume change of biomass particle i	$[L^3]$
ε	Porosity	—
ε_A	Areal porosity	—
λ_f	Equivalent thickness of biomass	[L]
λ_i	Equivalent thickness of biomass component i in the biofilm	[L]
μ^{max}	Maximum specific growth rate of micro organisms	$[T^{-1}]$
ρ_i	Specific mass of particulate species i	$[M_i L^{-3}]$
$\rho(\mathbf{x})$	Density of biomass at location $\mathbf{x}$	$[M L^{-3}]$
ϕ_{eq}	Equivalent diameter of a sloughed particle	[L]
F_{det}	Detachment speed function	$[L T^{-1}]$
L_f	Maximum biofilm thickness	[L]
$L_{f,ms}$	Average of L_f in the mature state period	[L]
$L_{f,ss}$	Average of L_f in the steady state period	[L]
L_{Ol}	Thickness of the oxygen-limited zone	[L]
L_{Sl}	Thickness of the substrate-limited zone	[L]
$M_{i,j}$	Mass of particulate species i in biomass particle j	$[M_i\,particle^{-1}]$
$\boldsymbol{n}(\mathbf{x})$	Vector normal to the biofilm/liquid interface surface at location $\mathbf{x}$	[dimensionless]
$N_{particles}$	Number of biomass particles in the biofilm	[particle]
observed Y_{SO}	The time average of the ratio of $R_{S,biofilm}$ and $R_{O,biofilm}$	$[M_S M_O^{-1}]$
PD_O	Penetration depth of oxygen	[L]
PD_S	Penetration depth of substrate	[L]
q_S^{max}	Maximum specific substrate uptake rate	$[M_S M_{\bar{X}}^{-1} T^{-1}]$
R_{det}	Total rate of biomass detachment $(R_{slo} + R_{ero})$	$[M L^2 T^{-1}]$
R_{ero}	Erosion rate	$[M L^2 T^{-1}]$
$R_{O,biofilm}$	Net oxygen consumption rate in the biofilm	$[M_O L^{-3} T^{-1}]$
$R_{S,biofilm}$	Net substrate consumption rate in the biofilm	$[M_S L^{-3} T^{-1}]$
R_{slo}	Sloughing rate	$[M L^2 T^{-1}]$
SRT	Solids retention time	[T]
t	Simulation time	[T]
$T(\mathbf{x})$	Time until detachment for a point located at position $\mathbf{x}$ inside the biofilm	[T]
t_{finish}	Finish simulation time	[T]
$\mathbf{x}$	Vector describing location is space, i.e. (x, y) for 2D, (x, y, z) for 3D	[L]

J.B. Xavier thankfully acknowledges financial support by the F.C.T./M.C.T.E.S., Portugal through grant SFRH/BPD/11485/2002. The authors also acknowledge Erik Alpkvist from Malmö University, Sweden, for introducing us to the level set method.

References

Alpkvist E, Overgaard NC, Gustafsson S, Heyden A. 2004. A new mathematical model for chemotactic bacterial colony growth. Wat Sci Technol 49(11–12):187–192.

Beuling EE, van den Heuvel JC, Ottengraf SPP. 2000. Diffusion coefficients of metabolites in active biofilms. Biotechnol Bioeng 67(1):53–60.

Beun JJ, Dircks K, Van Loosdrecht MCM, Heijnen JJ. 2002. Poly-beta-hydroxybutyrate metabolism in dynamically fed mixed microbial cultures. Water Res 36(5):1167–1180.

Boyd A, Chakrabarty AM. 1994. Role of alginate lyase in cell detachment of pseudomonas-aeruginosa. Appl Environ Microbiol 60(7):2355–2359.

Bryers JD. 1988. Modeling biofilm accumulation. In: Bazin MJ, Prosse JI, editors. Physiological models in microbiology. Boca Raton, FL: CRC Press. pp 109–104.

Bryers JD, Drummond F. 1998. Local macromolecule diffusion coefficients in structurally non-uniform bacterial biofilms using fluorescence recovery after photobleaching (FRAP). Biotechnol Bioeng 60(4): 462–473.

Chang I, Gilbert ES, Eliashberg N, Keasling JD. 2003. A three-dimensional, stochastic simulation of biofilm growth and transport-related factors that affect structure. Microbiology-SGM 149:2859–2871.

Characklis WG, Marshall KC, editors. 1990. Biofilms: A basis for an interdisciplinary approach. New York: Wiley Interscience. pp 3–15.

Choi YC, Morgenroth E. 2003. Monitoring biofilm detachment under dynamic changes in shear stress using laser-based particle size analysis and mass fractionation. Water Sci Technol 47(5):69–76.

Dockery J, Klapper I. 2001. Finger formation in biofilm layers. SIAM J Appl Mathe 62(3):853–869.

Eberl HJ, Parker DF, Van Loosdrecht MCM. 2001. A new deterministic spatio-temporal continuum model for biofilm development. J Theor Med 3(3):161–175.

Eberl HJ, Picioreanu C, Heijnen JJ, Van Loosdrecht MCM. 2000. A three-dimensional numerical study on the correlation of spatial structure, hydrodynamic conditions, and mass transfer and conversion in biofilms. Chem Eng Sci 55(24):6209–6222.

Hermanowicz SW. 2001. A simple 2D biofilm model yields a variety of morphological features. Mathe Biosci 169:1–14.

Horn H, Neu TR, Wulkow M. 2001. Modelling the structure and function of extracellular polymeric substances in biofilms with new numerical techniques. Water Sci Technol 43(6):121–127.

Horn H, Reiff H, Morgenroth E. 2003. Simulation of growth and detachment in biofilm systems under defined hydrodynamic conditions. Biotechnol Bioeng 81(5):607–617.

Horn H, Wasche S, Hempel DC. 2002. Simulation of biofilm growth, substrate conversion and mass transfer under different hydrodynamic conditions. Water Sci Technol 46(1–2):249–252.

Hunt SM, Hamilton MA, Sears JT, Harkin G, Reno J. 2003. A computer investigation of chemically mediated detachment in bacterial biofilms. Microbiology-SGM 149:1155–1163.

Kinner NE, Balkwill DL, Bishop PL. 1983. Light and electron mocroscopic studies of microorganisms growing in rotationg biological contactor biofilms. Appl Environ Microbiol 45:1659–1669.

Klapper I. 2004. Effect of heterogeneous structure in mechanically unstressed biofilms on overall growth. Bull Math Biol 66:809–824.

Kreft JU, Picioreanu C, Wimpenny JWT, Van Loosdrecht MCM. 2001. Individual-based modelling of biofilms. Microbiology-SGM 147: 2897–2912.

Kreft JU, Wimpenny JWT. 2001. Effect of EPS on biofilm structure and function as revealed by an individual-based model of biofilm growth. Water Sci Technol 43(6):135–141.

Kwok WK, Picioreanu C, Ong SL, Van Loosdrecht MCM, Ng WJ, Heijnen JJ. 1998. Influence of biomass production and detachment forces on biofilm structures in a biofilm airlift suspension reactor. Biotechnol Bioeng 58(4):400–407.

Laspidou CS, Rittmann BE. 2004. Modeling the development of biofilm density including active bacteria, inert biomass, and extracellular polymeric substances. Water Res 38(14–15):3349–3361.

Lewandowski Z, Beyenal H, Stookey D. 2004. Reproducibility of biofilm processes and the meaning of steady state in biofilm reactors. Wat Sci Technol 49(11):359–364.
Morgenroth E, Wilderer PA. 1999. Controlled biomass removal—The key parameter to achieve enhanced biological phosphorus removal in biofilm systems. Water Sci Technol 39(7):33–40.
Morgenroth E, Wilderer PA. 2000. Influence of detachment mechanisms on competition in biofilms. Water Res 34(2):417–426.
Noguera DR, Pizarro G, Clapp LW. 2000. Mathematical modeling of trichloroethylene (TCE) degradation in membrane-attached biofilms. Water Sci Technol 41(4–5):239–244.
Noguera DR, Pizarro G, Stahl DA, Rittmann BE. 1999. Simulation of multispecies biofilm development in three dimensions. Wat Sci Tech 39(7):503–510.
Picioreanu C, Kreft JU, Van Loosdrecht MCM. 2004. Particle-based multidimensional multispecies model. Appl Environ Microbiol 70(5): 3024–3040.
Picioreanu C, Van Loosdrecht MCM, Heijnen J. 1998. Mathematical modelling of biofilm structure with a hybrid differential-discrete cellular automaton approach. Biotech Bioeng 58(1):101–116.
Picioreanu C, Van Loosdrecht MCM, Heijnen JJ. 2000a. Effect of diffusive and convective substrate transport on biofilm structure formation: A two-dimensional modeling study. Biotechnol Bioeng 69(5):504–515.
Picioreanu C, Van Loosdrecht MCM, Heijnen JJ. 2000b. A theoretical study on the effect of surface roughness on mass transport and transformation in biofilms. Biotechnol Bioeng 68(4):355–369.
Picioreanu C, Van Loosdrecht MCM, Heijnen JJ. 2001. Two-dimensional model of biofilm detachment caused by internal stress from liquid flow. Biotechnol Bioeng 72(2):205–218.
Pizarro G, Griggeath D, Noguera DR. 2001. Quantitative cellular automaton model for biofilms. J Environ Eng 127(9):782–789.
Reichert P. 1994. Aquasim—A tool for simulation and data-analysis of aquatic systems. Water Sci Technol 30(2):21–30.
Rittmann BE, Schwarz AO, Eberl HJ, Morgenroth E, Perez J, van Loosdrecht M, Wanner O. 2004. Results from the multi-species Benchmark Problem (BM3) using one-dimensional models. Water Sci Technol 49(11–12): 163–168.
Sethian JA. 1996. A fast marching level set method for monotonically advancing fronts. Proc Natl Acad Sci USA 93(4):1591–1595.
Sethian JA. 1999. Fast marching methods. SIAM Rev 41(2):199–235.
Stewart PS. 1993. A model of biofilm detachment. Biotechnol Bioeng 41(1):111–117.
Tijhuis L, Hijman B, Van Loosdrecht MCM, Heijnen JJ. 1996. Influence of detachment, substrate loading and reactor scale on the formation of biofilms in airlift reactors. Appl Microbiol Biotechnol 45(1–2):7–17.
Van Loosdrecht MCM, Eikelboom D, Gjaltema A, Mulder A, Tijhuis L, Heijnen JJ. 1995. Biofilm structures. Water Sci Technol 32(8):35–43.
Van Loosdrecht MCM, Heijnen JJ, Eberl HJ, Kreft JU, Picioreanu C. 2002. Mathematical modelling of biofilm structures. Antonie van Leeuwenhoek 81:245–256.
Wanner O, Gujer W. 1986. A multispecies biofilm model. Biotech Bioeng 28:314–328.
Wanner O, Reichert P. 1996. Mathematical modeling of mixed-culture biofilms. Biotechnol Bioeng 49:172–184.
Wasche S, Horn H, Hempel DC. 2000. Mass transfer phenomena in biofilm systems. Water Sci Technol 41(4–5):357–360.
Wasche S, Horn H, Hempel DC. 2002. Influence of growth conditions on biofilm development and mass transfer at the bulk/biofilm interface. Water Res 36(19):4775–4784.
Xavier JB, Picioreanu C, van Loosdrecht M. 2004. A modelling study of the activity and structure of biofilms in biological reactors. Biofilms, in press.
Xavier JB, Picioreanu C, Van Loosdrecht MCM. 2005. A framework for multidimensional modelling of activity and structure of multispecies biofilms. Environ Microbiol, in press.
Yang X, Beyenal H, Harkin G, Lewandowski Z. 2000. Quantifying biofilm structure using image analysis. J Microbiol Meth 39:109–119.
Zhang XQ, Bishop PL. 2003. Biodegradability of biofilm extracellular polymeric substances. Chemosphere 50(1):63–69.